Bastian, N, Pfeffer, J, Kruijssen, JMD, Crain, RA, Trujillo-Gomez, S and Reina-Campos, M

 The globular cluster system mass-halo mass relation in the E-MOSAICS simulations

http://researchonline.ljmu.ac.uk/id/eprint/14044/

Article

For more information please contact researchonline@ljmu.ac.uk

The globular cluster system mass–halo mass relation in the E-MOSAICS simulations

Nate Bastian,[1][*] Joel Pfeffer [ID],[1] J. M. Diederik Kruijssen [ID],[2] Robert A. Crain [ID],[1]
Sebastian Trujillo-Gomez [ID][2] and Marta Reina-Campos [ID][2]

[1]*Astrophysics Research Institute, Liverpool John Moores University, 146 Brownlow Hill, Liverpool L3 5RF, UK*
[2]*Astronomisches Rechen-Institut, Zentrum für Astronomie der Universität Heidelberg, Mönchhofstrasse 12-14, D-69120 Heidelberg, Germany*

ABSTRACT

Linking globular clusters (GCs) to the assembly of their host galaxies is an overarching goal in GC studies. The inference of tight scaling relations between GC system properties and the mass of both the stellar and dark halo components of their host galaxies are indicative of an intimate physical connection, yet have also raised fundamental questions about how and when GCs form. Specifically, the inferred correlation between the mass of a GC system (M_{GC}) and the dark matter halo mass (M_{halo}) of a galaxy has been posited as a consequence of a causal relation between the formation of dark matter mini-haloes and GC formation during the early epochs of galaxy assembly. We present the first results from a new simulation of a cosmological volume ($L = 34.4$ cMpc on a side) from the E-MOSAICS suite, which includes treatments of the formation and evolution of GCs within the framework of a detailed galaxy formation model. The simulated M_{GC}–M_{halo} relation is linear for halo masses $> 5 \times 10^{11}$ M$_\odot$, and is driven by the hierarchical assembly of galaxies. Below this halo mass, the simulated relation features a downturn, which we show is consistent with observations, and is driven by the underlying stellar mass–halo mass relation of galaxies. Our fiducial model reproduces the observed M_{GC}–$M_\star$ relation across the full mass range, which we argue is more physically relevant than the M_{GC}–M_{halo} relation. We also explore the physical processes driving the observed constant value of $M_{GC}/M_{halo} \sim 5 \times 10^{-5}$ and find that it is the result of a combination of cluster formation physics and cluster disruption.

Key words: galaxies: star clusters: general.

1 INTRODUCTION

One of the main goals in stellar cluster research is to place globular clusters (GCs) and their young counterparts, young massive clusters (YMCs), in the wider context of galaxy assembly (see e.g. the recent reviews of Kruijssen 2014 and Forbes et al. 2018a). How do GCs trace the stellar component and dark halo mass of their host galaxy, and what drives these relations? A number of works have highlighted that GC populations obey scaling relations with the properties of their host galaxies, suggesting an intimate and causal relationship between the two (e.g. Peng et al. 2008; Georgiev et al. 2010). Particular attention has been placed on the relation between the mass of a GC population (M_{GC}) and that of the host galaxy's halo or virial mass (M_{halo} or M_{200}, which we use interchangeably). Observations show a near-linear scaling between the mass in these two quantities (e.g. Blakeslee, Tonry & Metzger 1997; Blakeslee 1999) with a proportionality factor $\eta = M_{GC}/M_{halo} \sim 5 \times 10^{-5}$ (e.g. Harris, Blakeslee & Harris 2017). At first glance, such a relation appears surprising, given that the more natural connection is expected to be that between the GCs and the stellar mass ($M_\star$) of the host, if GC formation is a natural consequence of star formation. Hence, the relation S_M ($=100 \times M_{GC}/M_\star$) versus $M_\star$ would be expected to encode more information about GC formation and their relation

to the host galaxy. Additionally, there exists a non-linear relation between the $M_\star$ and the inferred M_{halo} of galaxies (e.g. Behroozi, Wechsler & Conroy 2013; Moster, Naab & White 2013), rendering the apparently simple relation between M_{GC} and M_{halo} relation all the more surprising.

Some authors have taken the empirical M_{GC}–M_{halo} relation to conclude that GCs must have formed early on in the galaxy assembly process, before baryonic processes (e.g. feedback) cause the star formation rate (SFR) to deviate strongly from the gas inflow rate (see e.g. van de Voort et al. 2011). The implication would be that GCs are more directly tied to the dark matter of the host galaxy than the stars, forming in dark matter mini-haloes during the early epoch of galaxy assembly. For example, if a given mass of dark matter halo results in a fixed amount of mass/number of GCs to form, then the linear M_{GC}–M_{halo} relation would be a natural result (e.g. Boylan-Kolchin 2017). Within cosmological simulations, the number of independent dark matter mini-haloes that are capable of forming GCs but have not yet formed stars decreases strongly with decreasing redshift, implying that if mini-haloes were the preferential site of GC formation, most GCs must form before $z = 6$. However, there is growing evidence that GC formation is not restricted to the early Universe, and that they can form across all cosmic history, from very early times, to cosmic noon and even in the local Universe today (e.g. Holtzman et al. 1992; Schweizer & Seitzer 1998; Kruijssen 2015; Johnson et al. 2017; Vanzella et al. 2017; Reina-Campos et al. 2019; Usher et al. 2019).

[*] E-mail: N.J.Bastian@ljmu.ac.uk

An alternative explanation of the linear M_{GC}–M_{halo} relation was put forward by Kruijssen (2015), who argued that the combination of the physics of cluster formation and the preferential disruption of GCs based on their environment would result in a near-linear relation. The subsequent merging of galaxies (along with their GC populations) would then act to fully linearize the relation. A related interpretation has recently been put forward by El-Badry et al. (2019) and Choksi & Gnedin (2019). These authors suggest that the hierarchical growth of galaxies naturally leads to such a tight correlation, independent of the adopted cluster formation model, except at the low halo mass end, which may retain some memory of GC formation. Effectively, in this view, the M_{GC}–M_{halo} relation is a result of the central limit theorem, echoing the interpretation of the origin of scaling relations between central supermassive black holes (BHs) and galaxy properties advanced by Jahnke & Macciò (2011). In both the El-Badry et al. (2019) and Choksi & Gnedin (2019) works, the authors show that a GC formation model where clusters form throughout cosmic history can result in the observed M_{GC}–M_{halo} relation, without any explicit connection between the formation of GCs and dark matter (mini) haloes.

While these works were able to successfully explain the linear relation between the mass in GCs and that of the host halo, due to the lack of spatial resolution and baryonic physics in the models the authors were unable to explore the normalization of the relation. What physical processes are responsible for GCs to represent a near constant mass fraction of 0.005 per cent of their host galaxy? Is cluster formation or disruption the dominant process? If it is the former, what is the relative role of the shape of the cluster mass function and the cluster formation efficiency?

Observational studies have attempted to trace the M_{GC}–M_{halo} relation to ever lower halo masses in order to test if, and at what mass scale, the linear relation breaks down. Forbes et al. (2018b) have studied a heterogeneous sample of nearby dwarf galaxies to extend the relation down to $M_{halo} \sim 10^8$ M$_\odot$, and conclude that the relation continues to be linear down to at least this limit. This is in tension with the models of El-Badry et al. (2019) and Choksi & Gnedin (2019), which predict a downturn near $\sim 5 \times 10^{11}$ M$_\odot$. The origin of this discrepancy is not entirely clear – it is one of the goals of this paper to understand this difference. We note, however, that if galaxies without GCs are included in the Forbes et al. (2018b) sample, the running median of the M_{GC}–M_{halo} relation does show a downturn near $M_{halo} \sim 10^{10}$ M$_\odot$ (see Georgiev et al. 2010).

In this work, we study the M_{GC}–M_{halo} relation in the E-MOSAICS simulations of the coformation and evolution of GCs and their host galaxies in a fully cosmological framework (Pfeffer et al. 2018; Kruijssen et al. 2019a; Crain et al., in preparation). With these simulations, we can trace the build-up of full GC populations alongside their host galaxy and explore the role of various physical processes in setting their properties. Additionally, we can analyse the simulations directly (i.e. measuring the dark matter halo mass of each of the galaxies in the simulations) or consider observational proxies commonly used in the literature (i.e. measure the stellar mass of a galaxy and translate this to a halo mass using a scaling relation). This allows us to explore many of the underlying assumptions in observational studies of the M_{GC}–M_{halo} relation, as well as to investigate how it relates to other observed correlations between GC and galactic properties.

This paper is organized as follows. In Section 2, we introduce the simulations used throughout this work. In Section 3, we present the main results and interpretation from the simulations, namely the origin of the M_{GC}–M_{halo} relation, comparisons with observations, and other scaling relations like the M_{GC}–$M_\star$ relation. Finally, in Section 4 we discuss the results and present our conclusions.

2 THE E-MOSAICS SIMULATIONS

2.1 Simulation set-up

The E-MOSAICS (MOdelling Star cluster population Assembly In Cosmological Simulations within EAGLE) project is a suite of cosmological hydrodynamical simulations based on the EAGLE (Evolution and Assembly of GaLaxies and their Environments) galaxy formation model (Crain et al. 2015; Schaye et al. 2015) with a subgrid treatment of stellar cluster formation, evolution, and disruption (Kruijssen et al. 2011; Pfeffer et al. 2018). The physical ingredients of the subgrid stellar cluster models have been presented in detail in Pfeffer et al. (2018) and Kruijssen et al. (2019a) and we refer the interested reader to those papers for more details. In this work, we use a new suite of simulations, with the same physical model for cluster formation and evolution and at the same EAGLE resolution as in previous works, but instead of focusing on zoom-in simulations of Milky Way-mass haloes (Pfeffer et al. 2018; Kruijssen et al. 2019a) or a small periodic volume ($L = 12.5$ cMpc; Pfeffer et al. 2019), we use the simulation of a large periodic volume of 34.4 comoving Mpc (cMpc) on a side. This simulation has a volume 2.6 times larger than the previous largest EAGLE simulation at the same resolution (L025N0752) and will be presented in detail in Crain et al. (in preparation).

EAGLE is a suite of hydrodynamical simulations of galaxy formation in the Λ cold dark matter cosmogony (for full details, see Crain et al. 2015; Schaye et al. 2015). The simulations are evolved with a highly modified version of the N-body, smoothed particle hydrodynamics code GADGET3 (last described by Springel 2005), which include subgrid routines describing radiative cooling (Wiersma, Schaye & Smith 2009a), star formation (Schaye & Dalla Vecchia 2008), stellar evolution and mass-loss (Wiersma et al. 2009b), the seeding and growth of BHs via gas accretion and BH–BH mergers (Rosas-Guevara et al. 2015), and feedback associated with star formation and BH growth (Booth & Schaye 2009). The parameters describing the energy feedback from supernovae and active galactic nuclei are calibrated such that the simulations reproduce the present-day galaxy stellar mass function, size–mass relation of disc galaxies, and the relation between the mass of central BHs and galaxy stellar mass. The simulations were performed assuming a Planck Collaboration XVI (2014) cosmology, with $\Omega_m = 0.307$, $\Omega_\Lambda = 0.693$, $\Omega_b = 0.04825$, $h = 0.6777$, and $\sigma_8 = 0.8288$.

Coupled to the EAGLE model is the MOSAICS model describing the formation and evolution of star clusters (Kruijssen et al. 2011; Pfeffer et al. 2018). Star clusters are treated as a subgrid component of the stellar particles, such that they adopt the properties of the host particle (i.e. positions, velocities, ages, abundances) and form and evolve according to local properties within the simulation (namely the local ambient gas and dynamical properties). Cluster formation within the model is described by two main parameters, the cluster formation efficiency (CFE, the fraction of stars formed within bound clusters; Bastian 2008) and the upper exponential truncation to the Schechter (1976) cluster mass function ($M_{c,\star}$, with a power-law index of -2 at lower masses). The fiducial E-MOSAICS cluster formation model allows the CFE and $M_{c,\star}$ to vary as a function of the local environmental conditions; specifically we adopt the Kruijssen (2012) model for the CFE and the Reina-Campos & Kruijssen (2017) model for $M_{c,\star}$. Alternative cluster formation models were tested by adopting a constant CFE or a pure power-law mass function (discussed in further detail below). In order to reduce memory requirements for the simulations, only clusters with initial masses $>5 \times 10^3$ M$_\odot$ are evolved and we assume instant disruption for clusters formed with lower masses. Following their formation,

clusters may lose mass through stellar evolution (according to the EAGLE model), two-body relaxation depending on the strength of the local tidal field[1] and tidal shocks from rapidly changing tidal fields based on the derivations of Gnedin, Hernquist & Ostriker (1999), Prieto & Gnedin (2008), and Kruijssen et al. (2011). Star clusters that fall below a mass of 10^2 M$_\odot$ (through any mechanism) are assumed to be fully disrupted. Total removal of clusters via dynamical friction (assuming they merge to the centre of their host galaxy) is treated in post-processing and applied at every snapshot in the simulation (see Pfeffer et al. 2018).

The E-MOSAICS project aims to carry out self-consistent simulations of the coformation and evolution of galaxies along with their stellar cluster populations. Specifically, we are aiming to test whether the YMCs observed in nearby galaxies (as well as our own) share the same formation mechanisms as the ancient GCs. Using E-MOSAICS, we have carried out a number of studies that have attacked this problem from a variety of angles. For example, the simulations have been shown to reproduce the observed scaling relations for young massive clusters in nearby galaxies, including systematic variations in the cluster initial mass function and the fraction of stars that form in clusters as a function of environment (Pfeffer et al. 2019). They have been used to investigate the origin of the 'blue tilt' in GC populations without invoking multiple epochs of star formation (Usher et al. 2018), as well as the galaxy-to-galaxy scatter in the age–metallicity relation of GCs (Kruijssen et al. 2019a). The latter resulted in the inference of a previously unknown major accretion event during the early assembly of the Milky Way (Kruijssen et al. 2019b, 2020). Hughes et al. (2019) used the simulations to trace the build up of galaxy haloes (and their GC populations) using stellar streams of accreted satellites. They predict that GCs belonging to identifiable stellar streams should be, on average, younger than GCs located off streams, which has recently been observed in the M31 GC system (Mackey et al. 2019). Reina-Campos et al. (2019) used the simulations to show that, at least for Milky Way-like galaxies, the GC populations are expected to form across a wide range of redshifts, with a peak GC formation rate at $z \sim 2$. Finally, we have used the E-MOSAICS to quantify the amount of dynamical mass-loss experienced by GCs (Reina-Campos et al. 2018), allowing us to reproduce the fractions of the stellar bulge (Hughes et al. 2020) and stellar halo that are constituted by disrupted GCs (Reina-Campos et al. 2020). Given that the simulations are able to reproduce a broad range of observational properties (while also making explicit predictions for future observables) of both young stellar clusters and old GCs, we argue that the basic model adopted by E-MOSAICS (i.e. that the same underlying physical mechanisms govern cluster formation across cosmic history) is accurate and can be further applied to new regimes.

2.2 E-MOSAICS periodic volume

We conducted a simulation (L034N1034) of a periodic cube of size $L = 34.4$ cMpc on a side with the E-MOSAICS model. Full details of the simulation will be presented in Crain et al. (in preparation). Briefly, the simulation adopts the same subgrid physics as for the E-MOSAICS zoom-in simulations (Pfeffer et al. 2018; Kruijssen et al. 2019a). The simulation uses 2×1034^3 particles (with an equal

number of baryonic and dark matter particles), such that the dark matter particle mass is 1.21×10^6 M$_\odot$ and the initial gas particle mass is 2.26×10^5 M$_\odot$. The Plummer-equivalent gravitational softening length is fixed in comoving units to 1/25 of the mean interparticle separation (1.33 comoving kpc) until $z = 2.8$, and in proper units (0.35 pkpc) thereafter. The simulation was performed with the 'Recalibrated' EAGLE model (see Schaye et al. 2015), using a resolution identical to the L025N0752 volume, and thus achieves results for the galaxy population consistent with the EAGLE Recal-L025N0752 simulation. In total, 29 snapshots and 405 'snipshots' were saved between redshifts $z = 20$ and $z = 0$ (spaced approximately linearly in scale factor).

Unlike the previous E-MOSAICS simulations, which reran simulations with different cluster formation physics (see Pfeffer et al. 2018), for the L034N1034 simulation we ran all four cluster formation models (Section 2.3) in parallel. This is possible since the EAGLE galaxy formation model is independent of the MOSAICS star cluster model. Once formed, all star clusters are then evolved following the same cluster evolution model according to their local tidal field (Section 2). We note that it is necessary to run the MOSAICS model on the fly, because the variation of the local tidal field at the position of each cluster must be followed at a time resolution of <1 Myr, which is much finer than the computationally feasible output interval of simulation snapshots.

Galaxies (subhaloes) were identified in the simulation using the method described in Schaye et al. (2015). Dark matter structures were first identified using the friends-of-friends (FoF) algorithm (Davis et al. 1985) with a linking length 0.2 times the mean interparticle separation. Gravitationally bound substructures (galaxies and subhaloes) were then identified using the SUBFIND algorithm (Springel et al. 2001; Dolag et al. 2009). Within each FoF group, the galaxy that contains the particle with the lowest value of the gravitational potential is considered to be the *central* galaxy, and all other galaxies are considered to be *satellite* galaxies. Stellar particles (and the star clusters they host) are thus allocated to galaxies by the SUBFIND binding criteria. At $z = 0$, the volume has [465, 69, 7] haloes with $M_{200} > [10^{11}, 10^{12}, 10^{13}]$ M$_\odot$.

2.3 Alternate cluster formation models

In order to explore the effect of GC formation physics on the resulting $M_{GC}-M_{halo}$ relation, we follow Reina-Campos et al. (2019, hereafter RC19) who investigated the four different E-MOSAICS cluster formation models, which are outlined below as well as in Table 1.

Table 1. Cluster formation models considered in this work. From left to right, columns contain the name of the cluster formation scenario and the description used for the CFE and the ICMF, respectively.

Name	CFE	ICMF
Fiducial	$\Gamma(\Sigma, Q, \kappa)$ Kruijssen (2012)	Schechter function ($\alpha = -2$) and $M_{cl,max}(\Sigma, Q, \kappa)$ Reina-Campos & Kruijssen (2017)
CFE only	$\Gamma(\Sigma, Q, \kappa)$ Kruijssen (2012)	Power law of index $\alpha = -2$
$M_{c,\star}$ only	$\Gamma = 10$ per cent	Schechter function ($\alpha = -2$) and $M_{cl,max}(\Sigma, Q, \kappa)$ Reina-Campos & Kruijssen (2017)
No formation physics	$\Gamma = 10$ per cent	Power law of index $\alpha = -2$

---

[1]Following Gieles & Baumgardt (2008), we have added a term to the mass-loss rate from two-body relaxation to account for 'isolated' clusters, i.e. those in a weak tidal field. This change has only a minor influence, mainly for clusters with masses $\lesssim 10^4$ M$_\odot$.

(i) **Fiducial model:** This is our default model of which the CFE (Γ) and the truncation mass of the Schechter initial cluster mass function (ICMF) vary as a function of the properties of the local environment where the stars/clusters are forming.

(ii) **CFE only:** This was referred to as the '$\alpha = -2$' model in RC19. In this model, the ICMF is invariant as a pure power-law function with an index of -2, although it is sampled stochastically. The CFE, like in the fiducial model, varies with the local environment.

(iii) **M$_{c,\star}$ only:** This was referred to as the '$\Gamma = 10$ per cent' model in RC19. This model sets the CFE at a constant level (10 per cent) and allows the truncation mass ($M_{c,\star}$) of the ICMF to vary as in the fiducial model.

(iv) **No formation physics:** In this model, both the CFE and the ICMF are invariant (fixed at 10 per cent and a pure power law with an index of -2, respectively).

2.4 Analysis

We focus most of our analysis on central galaxies, because satellite galaxies can have their dark matter haloes (and GC populations) significantly affected by interactions with the central host. Most observational studies use scaling relations to infer the dark matter halo mass from the observed stellar mass, which are calibrated primarily on central galaxies, implying that the inclusion of satellites from our models would not be consistent. We limit our analysis to well-resolved galaxies with stellar masses $>10^8$ M$_\odot$ ($\gtrsim 500$ stellar particles), similar to the galaxy mass limit in Peng et al. (2008). At $z = 0$, this gives us a sample of 992 central galaxies, and 1707 galaxies in total when including satellites.

We refer to Appendix A for details on how the GC sample was selected in this work, as well as on how this affects the results. Briefly, we determine the total mass of the GC population using the top two decades of the present-day GC mass function for each galaxy.

3 RESULTS

3.1 The M_{GC}–M_{halo} relation

3.1.1 The shape of the relation

The M_{GC}–M_{halo} relation from the E-MOSAICS volume is shown in Fig. 1 for the fiducial model and for the three alternative cluster formation physics models in the left-hand panels. Additionally, horizontal lines show the estimated value of η from three observational studies, namely Spitler & Forbes (2009, S&F09; dash dotted line), Hudson, Harris & Harris (2014, H14; dotted line), and Harris et al. (2017, H17; dashed line). While the E-MOSAICS simulations do not invoke any direct relation between the dark matter halo of the galaxy and the number (or mass) of GCs within it, we see that for all models the M_{GC}–M_{halo} relation is linear above a halo mass of $\sim 5 \times 10^{11}$ M$_\odot$. This is consistent with the models of El-Badry et al. (2019) and Choksi & Gnedin (2019) who found that this linear behaviour is driven by the hierarchical build up of galaxies (essentially the central limit theorem) and is not tied to the formation of GCs nor their connection to dark matter. As we find the same behaviour in all of our models, regardless of the cluster formation physics included, our results are consistent with the conclusions of these authors, namely that the observed M_{GC}–M_{halo} relation does not imply a causal relation between dark matter and GCs.

However, like El-Badry et al. (2019) and Choksi & Gnedin (2019), we also find a downturn in the relation at lower halo masses, with the exact location sensitive to the adopted physics. In addition, we

see that the normalization of the relation is also a strong function of the adopted physics. These aspects are discussed in more detail in the following sections.

3.1.2 The normalization of the relation

While all of our simulations find a close to linear M_{GC}–M_{halo} relation above a certain halo mass, regardless of the adopted formation physics, we see that the normalization of the relation is dependent on the adopted model. In the rest of the discussion, we will only focus on the linear part of the relation in our simulations. For our fiducial model, we find a median η value that is in good agreement with S&F09 and slightly higher than H14 and H17. This slight overabundance of GCs may be caused by the underdisruption of metal-rich GCs within the E-MOSAICS simulations and we point the interested reader to Kruijssen et al. (2019a, appendix D) for a detailed discussion of this point.

The simulations using other formation physics models are systematically offset from the observed value of η. If $M_{c,\star}$ is fixed (i.e. a pure power-law cluster initial mass function with no truncation) and the CFE is allowed to vary, we end up producing too many GCs. If instead we adopt a constant CFE (10 per cent) and allow $M_{c,\star}$ to vary, we underestimate η, meaning that we do not produce enough GCs. The former effect is dominant, because using a constant CFE in combination with a power-law ICMF leads to the overprediction of η. Hence, while the hierarchical build up of galaxies naturally leads to a linear M_{GC}–M_{halo} relation for $\sim L^\star$ galaxies and above, independently of the input GC formation physics, the normalization of the relation does encode important information on the physics of GC formation.

We also investigate the role of cluster disruption on the normalization of the M_{GC}–M_{halo} relation. In Fig. 2, we show the relation with the present-day halo mass but now for the initial masses of GCs (i.e. before mass- through stellar evolution and cluster disruption). The overall shape of the distribution is similar, with the turndown at the same halo mass, but now the normalization is a factor of ~ 10 higher than observed. Including GC mass-loss (and full disruption) moves the high-mass end on to the observed relation and flattens the overall relation. This is due to GC disruption being more efficient in higher mass galaxies than less massive counterparts. We conclude that cluster disruption plays a strong role in setting the normalization of relation (as predicted by Kruijssen 2015), and models that neglect mass-loss (or only include secular mass-loss and neglect tidal shocks) will either overpredict η at $z = 0$ or, if calibrated at $z = 0$, will predict less evolution with redshift than models that do include cluster disruption.

3.2 Cause and implications of the downturn at low mass

An important feature visible in the top left panel (fiducial model) of Fig. 1 is that below a halo mass of 5×10^{11} M$_\odot$ the M_{GC}–M_{halo} relation begins to deviate from being linear. As discussed in Section 1, this appears to be in tension with observations that have not detected such a downturn to date Forbes et al. (2018b, hereafter F18). However, this downturn is a consistent prediction of models for the GC population, as it is also seen in the models of El-Badry et al. (2019) and Choksi & Gnedin (2019). In particular, El-Badry et al. (2019) find that this downturn is due to the lower gas surface densities and higher mass-loss rates of lower mass galaxies. As a result, both their fiducial model and ours produce fewer clusters at low gas surface densities.

We can demonstrate this in our model by considering the results for models with different cluster formation physics. In particular,
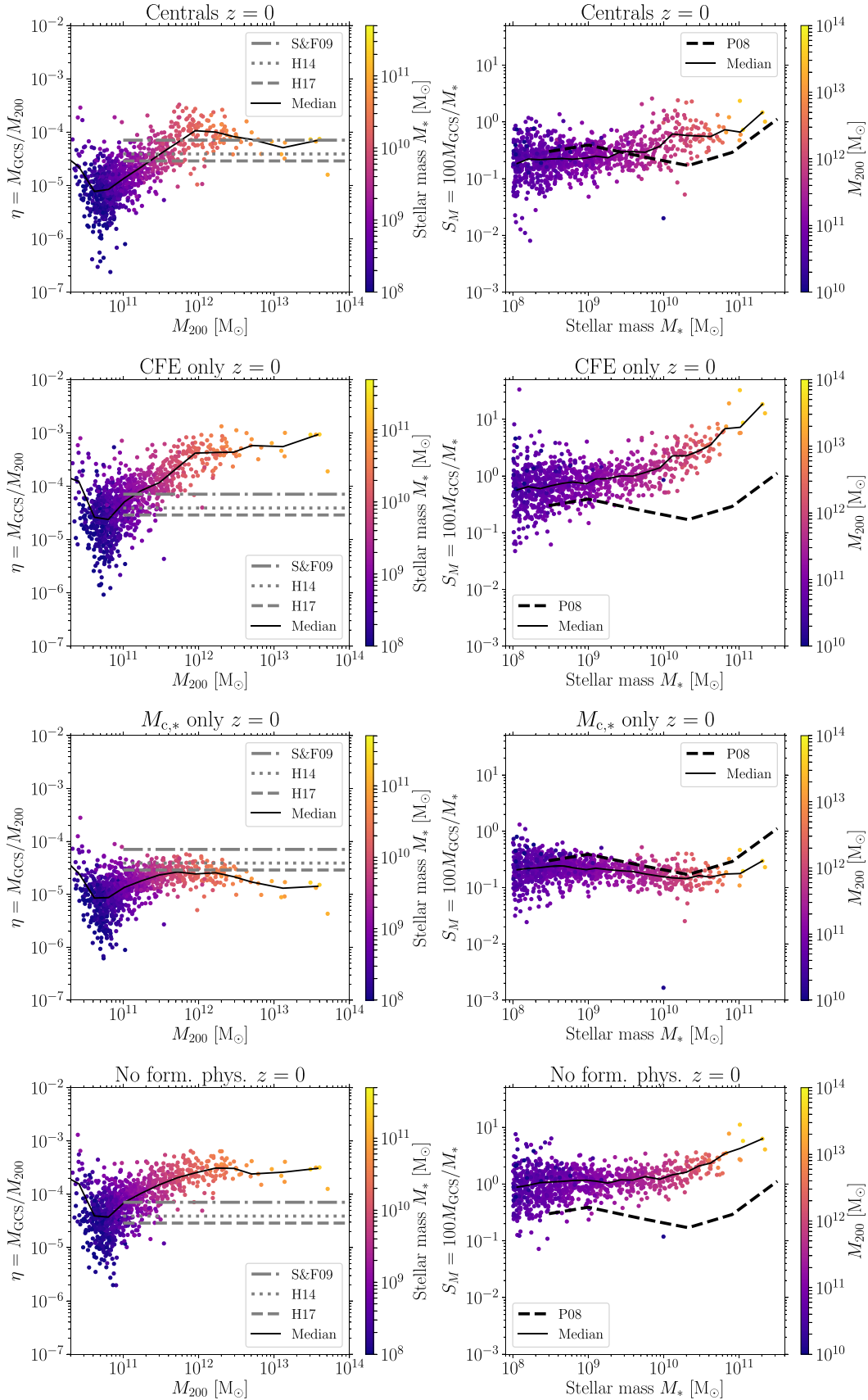
Figure 1. The $M_{\rm GC}$–$M_{\rm halo}$ (left-hand panels) and $S_{\rm M}$–$M_\star$ (right-hand panels) relations for galaxies within our simulation. See Table 1 for a summary of the differences between the simulations. The solid lines show the running median while the dashed, dotted, and dash–dotted lines show observational results from the literature (see text for details), which are restricted to halo masses $\gtrsim 10^{11}$ M$_\odot$.
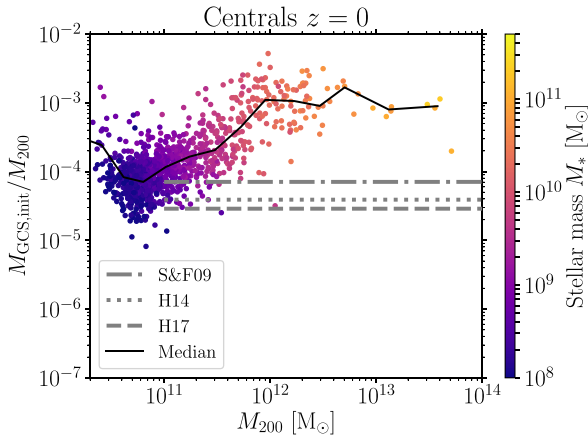
Figure 2. 'Initial' η versus M_{200}, obtained using the initial masses of the clusters. The flat (linear) relation is still evident above 5×10^{11} M$_\odot$, which is due mainly to the hierarchical assembly of galaxies. However, the normalization increases by a factor of 15 at high halo masses and by a factor of 10 at low masses, which causes this relation to be somewhat steeper than the one including cluster dissolution.

Fig. 1 shows that fixing the CFE to a constant value results in a flatter distribution, although there is still a downturn at low halo masses. In order to retain a flat distribution at lower values of M_{halo}, we would need to increase the CFE towards lower mass galaxies, which would be contrary to the adopted model and also inconsistent with the observed CFEs in nearby dwarf galaxies in the Universe today (e.g. Cook et al. 2012; Adamo & Bastian 2018).

Even when adopting a constant CFE, there is still a downturn at low galaxy masses. This is driven by the shape of the $M_\star$–M_{halo} relation of the parent galaxies, as this relation is rapidly changing below $M_{halo} \sim 5 \times 10^{11}$ M$_\odot$ (e.g. Behroozi et al. 2013; Moster et al. 2013; Schaye et al. 2015). Adopting a shallower $M_\star$–M_{halo} relation than that found in the EAGLE simulations could, in principle, flatten the resulting M_{GC}–M_{halo} relation (see Section 3.5).

In the right-hand panels of Fig. 1, we show the total amount of mass in GCs compared to the stellar mass ($M_\star$) of each galaxy. Additionally, the observational results from Peng et al. (2008) are shown as a dashed line. In this space, we find that our simulations follow the observations relatively well, and do not display any distinctive feature at the low stellar mass end, which is consistent with the observations. In our simulations, cluster formation and evolution is more closely tied to the formation of the stellar mass of the host galaxy than the dark matter halo or virial mass, and the ability of the simulations to reproduce the observed trend between GCs and the stellar mass suggests that the models are capturing much of the essential physics. The possible failure in reproducing the trend at low halo masses between the halo and GC system masses may rather reflect differences in relating M_{halo} to $M_\star$, as $M_\star$ is the more directly measurable quantity. This is discussed in more depth in Section 3.6.

3.3 Centrals versus satellites

So far, we have focused our attention on central galaxies, as the majority of observational work either focused directly on centrals or uses $M_\star$–M_{halo} relations that are built from observations of central galaxies (e.g. H17). In Fig. 3, we show the M_{GC}–M_{halo} relation for our sample of central galaxies (blue dots) as well as a sample of satellite galaxies (orange dots). We also show the running medians
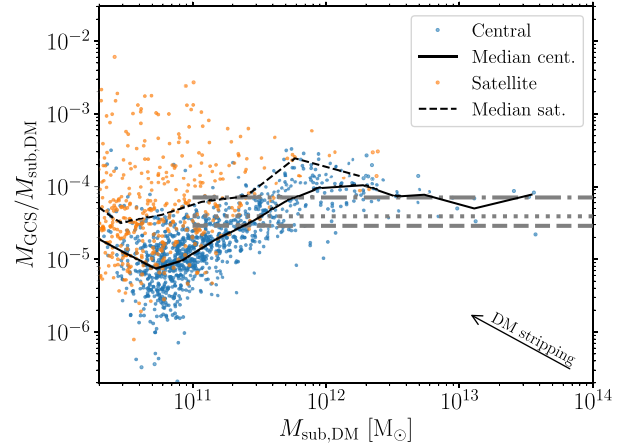

Figure 3. The M_{GC}–M_{halo} relation for central (blue) and satellite (orange) galaxies. We also show the median relations for central (solid lines) and satellite (dashed lines). Stripping of the dark matter halo (which happens much earlier than stripping of the stellar or GC component of the galaxies) causes the satellite population to scatter up and to the left in the figure. The use of a one-to-one conversion of stellar to halo mass based on central galaxies will lead to the overestimation of the actual halo mass for satellite galaxies.

of each distribution of centrals and satellites as a solid and dashed black line, respectively.

From Fig. 3, it is clear that at a fixed halo mass, satellite galaxies have a larger $\eta = M_{GC}/M_{halo}$ ratio, which is particularly noteworthy for halo masses less than $\sim 5 \times 10^{11}$ M$_\odot$. This is due to the tidal stripping of the satellite galaxy's dark matter halo by their central galaxy, causing the affected satellites to move to the upper left of the figure. This differential effect of tidal stripping occurs because the dark matter haloes of galaxies are spatially more extended than their GC populations.

F18 have investigated the M_{GC}–M_{halo} relation in a sample of nearby galaxies, using rotation curves to measure the dynamical mass of the galaxy halo. These authors report that the M_{GC}–M_{halo} relation remains linear (i.e. does not show a pronounced downturn) down to a halo mass of $\sim 10^8$ M$_\odot$.[2] However, the F18 sample contains a number of satellite galaxies (in particular at low masses). As shown in Fig. 3, this is expected to lead to a flatter M_{GC}–M_{halo} relation. We will return to this point in Section 3.5.

3.4 Redshift dependence

Choksi & Gnedin (2019) have used their model for GC formation and evolution within galaxies to trace the evolution of the M_{GC}–M_{halo} relation from a redshift of 10 until today. In their model, the shape of the relation is already set at $z = 10$ and the normalization evolves slowly from $z = 10$ to $z = 3$ (by a factor of ~ 2). Between $z = 3$ and $z = 0$, the shape of the relation still remains the same, but the evolution of the normalization accelerates as it decreases by a factor of ~ 10. The authors find that this rapid change is driven primarily by the build up of halo mass from $z = 3$ to $z = 0$, as the GC system mass remains largely constant, reflecting a rough balance between dynamical GC disruption and late GC formation and accretion.

---

[2]Although if galaxies without detected GCs are included the running mean/median would show a significant downturn below a halo mass of $\sim 10^{10}$ M$_\odot$.
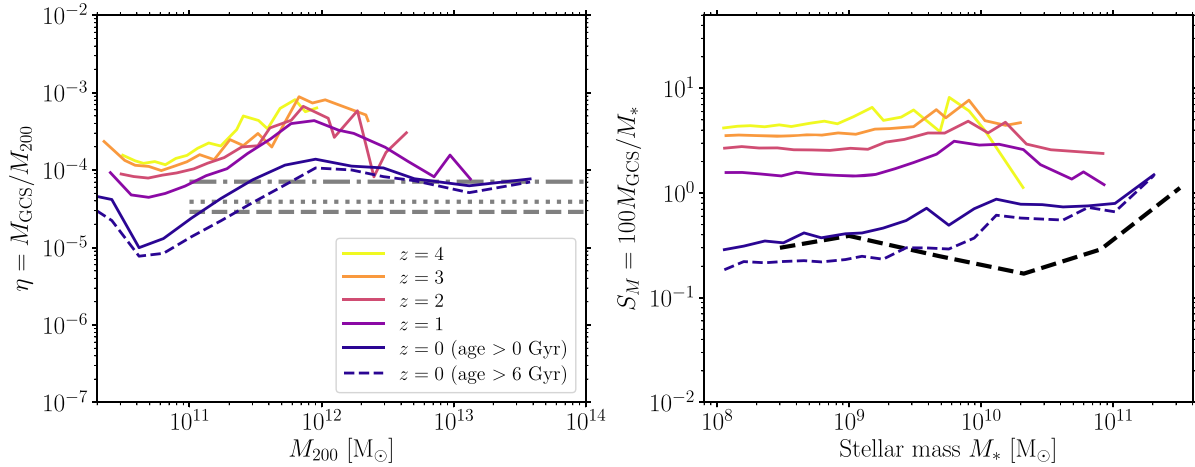
Figure 4. The median M_{GC}–M_{halo} relation (left-hand panel) and the median S_M–$M_\star$ relation (right-hand panel) for central galaxies at different redshifts, for the fiducial model. The M_{GC}–M_{halo} relation is set early on (at $z > 4$) and exhibits little evolution to $z \sim 1$, after which the relation evolves considerably to $z = 0$. We also show the $z = 0$ relation for two different GC age cuts, >6 Gyr (dashed line) and for all ages. Their similarity argues for a minor contribution of late-time GC formation to this relation. A similar conclusion is reached for the S_M–$M_\star$ relation (right-hand panel), for which we also show the observed relation from Peng et al. (2008) (long dashed black line).
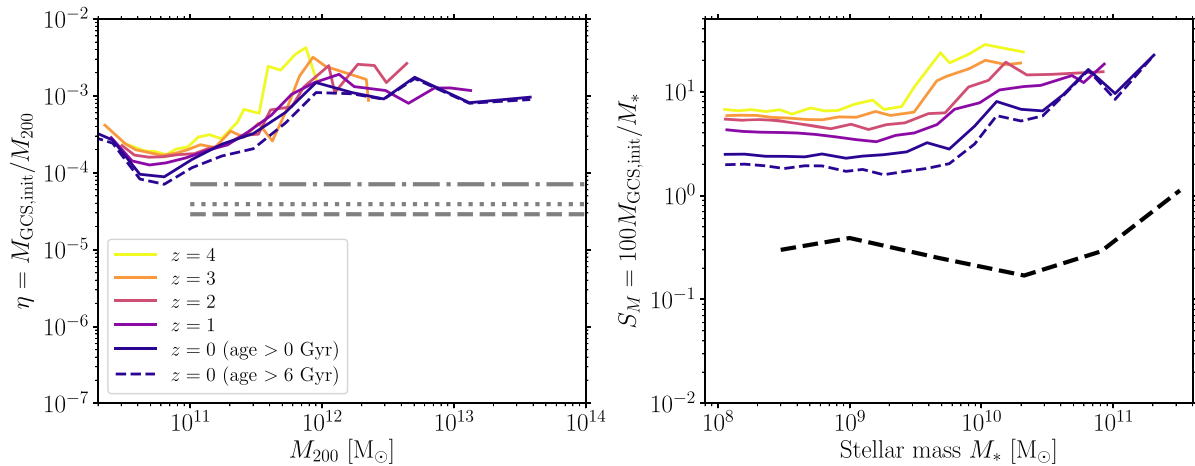

Figure 5. The same as Fig. 4, but calculating M_{GC} using the initial cluster masses (M_{halo} is the same for each galaxy as shown previously). The similarity in the M_{GC}–M_{halo} relation (when initial cluster mass is used) at all redshifts shows that cluster dissolution is the driving cause behind the M_{GC}–M_{halo} relation's evolution with redshift. For the S_M–$M_\star$ relation, the evolution with redshift (when initial cluster masses are used) is a reflection of formation bias, where galaxies that reach a certain stellar mass earlier did so through a higher mean SFR than galaxies that reach that mass later. More intense bursts of star formation leads to a higher fraction of the stellar mass in GCs.

In the left-hand panel of Fig. 4, we show the median M_{GC}–M_{halo} relation as a function of redshift for our model galaxies. Like Choksi & Gnedin (2019), we find that the overall shape of the relation is set at early times ($z > 4$ in our simulations) and evolves slowly to a redshift of ∼1, followed by a rapid drop to $z = 0$. Quantitatively, we predict a drop of a factor of ∼7–10 from $z = 2$ to $z = 0$, in good agreement with the results of Choksi & Gnedin (2019). For $z = 0$, we show the results for two different GC age cuts. One line shows all GCs (solid purple line), whereas the other only includes GCs older than 6 Gyr at $z = 0$ (dashed purple line). The similarity of the two relations, especially at large halo masses, suggests that late-time GC formation is a relatively minor driver of the normalization of this relation.

In order to find the origin of the redshift dependence of the M_{GC}–M_{halo} relation, in Fig. 5 we show the same relations, but now using the cluster initial masses. When the initial masses are used, we see little

evolution with redshift, hence it appears that cluster disruption is the driving cause of the redshift evolution in the simulations (as predicted by Kruijssen 2015).[3] Fig. 5 also shows the effects of formation bias, i.e. that galaxies that form early through intense bursts of star and cluster formation have a higher fraction of their mass in GCs than galaxies that grow to the same mass more gradually through cosmic history (e.g. Mistani et al. 2016; Kruijssen et al. 2019a). For example, a galaxy with $M_\star = 10^9$ M$_\odot$ at $z = 4$ has nearly three times the mass in GCs than the same mass galaxy at $z = 0$. Formation bias within the

---

[3]While the E-MOSAICS simulations likely underpredict the rate of cluster dissolution (see Kruijssen et al. 2019a), by concentrating our analysis on the high-mass end of the GC mass function the effect should be minimized.
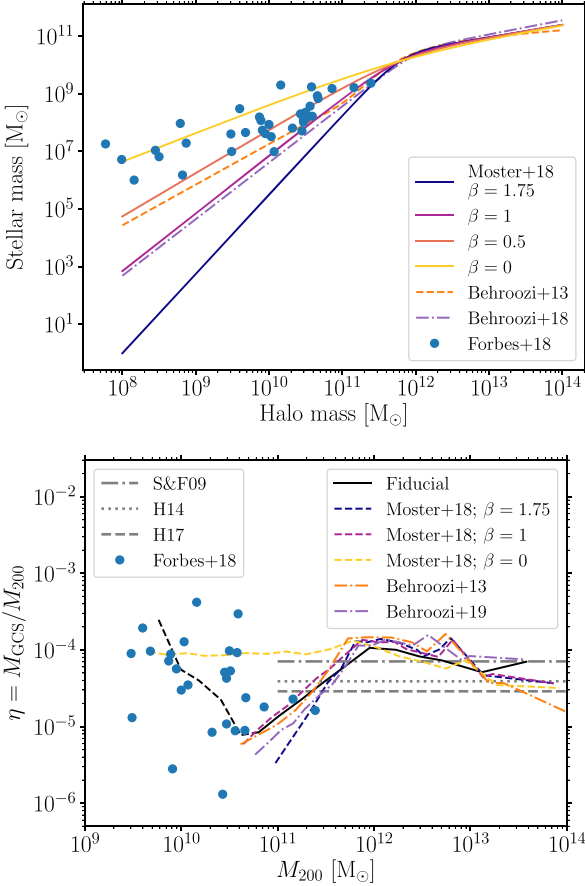
Figure 6. Top panel: The $M_\star$–M_{halo} relation of galaxies from a variety of sources. For the Moster et al. (2018) relation, we show the result of varying the slope of the low-mass end. The measurements (for galaxies that contain GCs) from F18 are shown as solid circles, and lie significantly above the more canonical relations in the literature. Bottom panel: The resulting M_{GC}–M_{halo} relation for our fiducial model when translating our M_{GC}–$M_\star$ relation using the stellar/halo mass relations from the top panel. Depending on the adopted $M_\star$–M_{halo} relation, the M_{GC}–M_{halo} relation may display a distinct and steep downturn or even remain flat (this can only be achieved by setting $\beta = 0$, implying $M_\star \propto M_{halo}$). The dashed black line shows our fiducial model below a halo mass of 5×10^{10} M$_\odot$), which begins to increase due to our imposed stellar mass cut (10^8 M$_\odot$, see text for details).

E-MOSAICS simulations will be explored in more detail in Crain et al. (in preparation).

In the right-hand panel of Fig. 4, we show the S_M versus $M_\star$ relation from our simulations at different redshifts. Additionally, the black dashed line shows the Peng et al. (2008) relation for observed galaxies at $z = 0$. We find a similar, albeit more gradual evolution of the relation as the M_{GC}–M_{halo} relation, suggesting that the stellar mass of the host galaxy is also growing from $z = 2$ to $z = 0$ without an appreciable change in GC system mass.

In the context of Figs 4 and 5, we note that El-Badry et al. (2019) additionally investigated a 'pathological' model, in which the mass in GCs is uncorrelated to that of the mass of the halo. In this type of model, reproducing the $z = 0$ M_{GC}–M_{halo} relation requires the opposite redshift evolution of that seen in our models, such that η at fixed halo mass is lower at higher redshift. Future observations with *JWST* or the E-ELT of GC populations as a function of redshift may be able to test these predictions.

By contrast, the fiducial model of El-Badry et al. (2019) shows a much milder evolution with redshift than both this study and that of Choksi & Gnedin (2019). For their fiducial model, El-Badry et al. find that the normalization of the M_{GC}–M_{halo} relation changes by only a factor of ~ 3 between $z = 3$ and $z = 0$. This weaker evolution, in contrast to the model presented here, may be a result of the lack of cluster disruption in the El-Badry et al. simulations. Hence, in order to reproduce the $z = 0$ relation with little or no disruption, it is necessary to have less evolution of the relation towards higher redshift (see Section 3.1.2). In this context, we note that the overall GC formation history in the model of El-Badry et al. (2019) is similar to that of E-MOSAICS (RC19).

3.5 Linking GC populations, stellar content, and halo mass of galaxies

In the majority of observational work on the M_{GC}–M_{halo} relation, the dark matter content of each galaxy was not measured directly, but rather was inferred from scaling relations between the stellar mass and the dark halo mass obtained from abundance matching or weak lensing surveys. While the $M_\star$–M_{halo} relation is relatively well constrained at high halo masses ($M_{halo} > 10^{11}$ M$_\odot$), below this mass differences between studies can amount to two orders of magnitude or more in the stellar mass at fixed halo mass. This uncertainty can have a large and important impact on the inferred M_{GC}–M_{halo} relation when translating from the observational plane of M_{GC}–$M_\star$.

Two exceptions to the above are the studies of Forbes et al. (2016) and F18, who used dynamical tracers to estimate the halo mass (although correction factors for each galaxy needed to be applied to extrapolate from the outermost dynamical measurement to M_{200}). In particular, F18 attempted to trace the M_{GC}–M_{halo} relation down to low halo masses to see whether the observed linear relation at high masses continues, or if a break appears in the relation. As discussed in the introduction and Section 3.3, the authors report that the relation (at least for galaxies that host GCs) continues to be linear down to at least $M_{halo} \sim 10^8$ M$_\odot$. This is in apparent contradiction to the predicted M_{GC}–M_{halo} relation found in our simulations, which features a notable downturn at $M_{halo} = 5 \times 10^{11}$ M$_\odot$.

For each of the galaxies in their sample, F18 measured M_{GC}, $M_\star$, and M_{halo}. As noted by the authors, their derived $M_\star$–M_{halo} relation is strongly inconsistent with the relation inferred through abundance matching, as well as empirical studies and simulations. Specifically, the results of F18 imply stellar masses $>1-2$ orders of magnitude larger[4] (at a halo mass of 10^9 M$_\odot$) than more canonical relations.

In the top panel of Fig. 6, we show the $M_\star$–M_{halo} relation as measured by Behroozi et al. (2013, 2019). Additionally, we show the Moster, Naab & White (2018) relation who adopt a double power-law formulation, with a low-mass slope, β, for which we show values in the range $\beta = 0-1.75$. The value preferred by Moster et al. (2018) is $\beta = 1.75$ at redshift 0 (the blue, lowest, line). We also show the individual data points from F18, which below a halo mass of $\sim 10^{11}$ M$_\odot$ are significantly above the canonical relations. If parametrized in the same way as done in Moster et al. (2018), the Forbes et al. data would imply $0 < \beta < 1$, significantly shallower than other studies.

These differences have important implications when translating into the M_{GC}–M_{halo} plane. In the bottom panel of Fig. 6, we show the resulting M_{GC}–M_{halo} relation, derived from our fiducial model using

---

[4]This is not due to the uncertainty in $M_\star$, but is instead caused by the large uncertainty in the inference of M_{halo} using dynamical models.

the median S_M–$M_\star$ relation from the top right panel of Fig. 1 and the different $M_\star$–M_{halo} relations shown in the upper panel. The solid line shows the relation directly measured in our fiducial simulation. Other lines show the resulting relation when adopting different $M_\star$–M_{halo} relations shown in the top panel. The solid points are the measurements for the galaxies from F18 shown in the top panel.

The dashed black line in the bottom panel of Fig. 6 shows the results of our fiducial model where it begins to increase due to our imposed stellar mass cut (10^8 M$_\odot$ – corresponding to a halo mass of 5×10^{10} M$_\odot$). Below this halo mass (due to the fixed stellar mass cut), we are only sensitive to the most extreme galaxies in terms of the $M_\star/M_{halo}$ ratio. These galaxies are part of a biased subpopulation that tend to have larger GC populations than other galaxies at comparable halo masses, resulting in elevated η values. This may also be affecting observational work and can only be overcome through complete, volume limited, surveys.

The results in Fig. 6 show that for a given, observed S_M–$M_\star$ relation the resulting inferred M_{GC}–M_{halo} relation can show a distinct downturn or even be flat, depending on the adopted $M_\star$–M_{halo} relation. Hence, uncertainties in the shape of the $M_\star$–M_{halo} relation at low masses, as well as inconsistencies between observations and simulations, mean that, at present, the low-mass end of the M_{GC}–M_{halo} relation cannot be used to place strong constraints on our understanding of GC formation and/or evolution.

We further investigate the importance of the $M_\star$–M_{halo} by looking at two observational samples that use M_{GC} and $M_\star$. The first is the median relation from Peng et al. (2008), which is shown as a dashed line in the right-hand panels of Fig. 1. The second is the F18 sample, where we adopt their measured M_{GC} and $M_\star$ i.e. we do not use their inferred M_{halo} values. Using these data sets, we then apply two commonly adopted $M_\star$–M_{halo} relations from the literature, namely those of Moster et al. (2018, with $\beta = 1.75$) and Behroozi et al. (2013).

The resulting, observationally inferred M_{GC}–M_{halo} relations are shown in Fig. 7. In the upper panel, we adopt the Behroozi et al. (2013) relation while in the lower panel we adopt the Moster et al. (2018) relation. Rather than appearing as a flat continuation from the results obtained for higher mass galaxies (shown as horizontal lines), both the Peng et al. (2008) and F18 data show a clear downturn at or near the same mass found in our simulations (i.e. $M_{halo} \sim 5 \times 10^{11}$ M$_\odot$). Again, we note that the simulations of El-Badry et al. (2019) and Choksi & Gnedin (2019) found a downturn at a similar mass.

We conclude that the observations of GC systems to date are consistent with the downturn in the M_{GC}–M_{halo} relation predicted in our model (within the large uncertainties in halo masses of low-mass galaxies). This downturn is not driven by the physics of GC formation or evolution, but rather is a simple reflection of the $M_\star$–M_{halo} relation as a function of halo mass. Hence, until the $M_\star$–M_{halo} relation at the low-mass end is pinned down, and the origin of the discrepancy between the relations seen in observations and simulations is known, the shape of the M_{GC}–M_{halo} relation at the low-mass end will tell us little about how GCs relate to their host galaxies or when and where they formed.

3.6 S_M–$M_\star$ relation

As noted above, in most observational studies, the halo mass of the host galaxy is not directly measured, but rather it is inferred, often through the assumption of a single relation to translate $M_\star$ to M_{halo} (notable exceptions to this are Forbes et al. 2016 and F18 discussed above). Hence, the M_{GC}–M_{halo} relation is not a direct relation, but contains two components. The first is the M_{GC}–$M_\star$ relation and
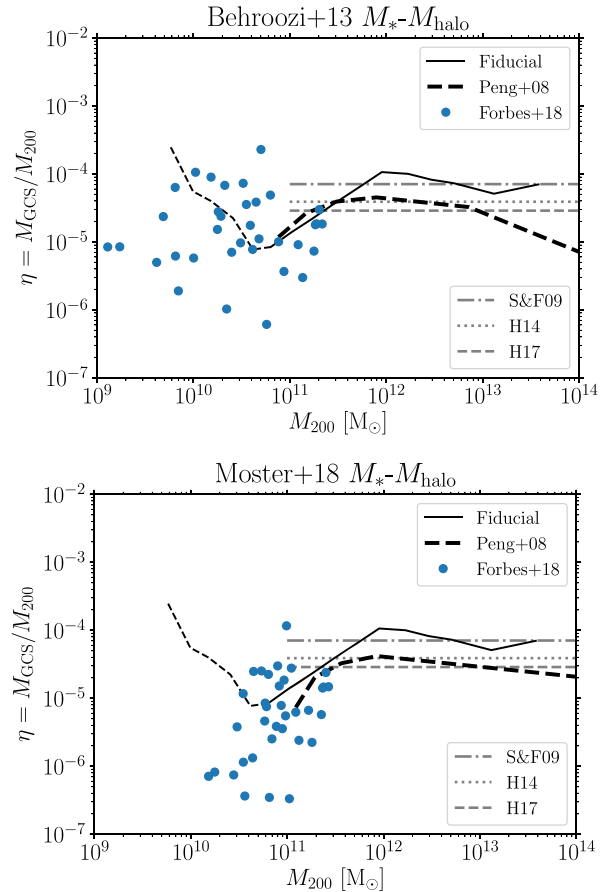

Figure 7. Top panel: The M_{GC}–M_{halo} relation inferred from the observed S_M–$M_\star$ relation from Peng et al. (2008) (dashed line), and F18 (filled circles) by adopting the Behroozi et al. (2013) $M_\star$–M_{halo} relation. Additionally, we show the results from our fiducial model as a solid line. Bottom panel: The same as the top figure but now adopting the Moster et al. (2018) $M_\star$–M_{halo} relation. Note that in both cases, the observations show a downturn at or near the same halo mass ($\sim 5 \times 10^{11}$ M$_\odot$) as our simulations. From this we conclude that, given the uncertainty in the $M_\star$–M_{halo} relation, the observed M_{GC}–M_{halo} relation is consistent with the relation found in the E-MOSAICS simulations.

the second is the $M_\star$–M_{halo} relation. This double dependence can make it difficult to isolate the physical effects driving any relation between GCs and their host galactic dark matter halo. As such, it is more insightful to investigate relations between quantities that can be directly observed.

Additionally, we argue that the use of the number of GCs (N_{GC}), which is adopted in some observational studies as a substitute for M_{GC}, is not an ideal quantity as it can be strongly affected by observational selection effects. For example, studies of Local Group galaxies often include GCs with masses below 10^4 M$_\odot$ (e.g. F18) while studies of more distant systems are limited to clusters above a few 10^5 M$_\odot$ (e.g. H17). Similarly, quantities like the specific frequency (S_N, i.e. the number of clusters per unit galaxy luminosity) are known to exhibit extreme stochasticity in the limit of low numbers of GCs, such that a single GC (independent of its mass) in a low-luminosity galaxy results in a high value of S_N, producing a statistical rather than a physically driven upturn.

For these reasons, we argue that the most physically driven estimator of the richness of a GC population is the total mass in

GC per unit galaxy stellar mass, S$_M$ = 100 × $M_{GC}/M_\star$. While this quantity has historicaly been less commonly used in observational studies relative to S$_N$ or η, it has been explored in some studies (e.g. Georgiev et al. 2010).

In the right-hand panels of Fig. 1, we show S$_M$ versus $M_\star$ for our simulations. For the fiducial model, we find the S$_M$–$M_\star$ relation to be nearly flat (and hence the M_{GC}–$M_\star$ relation to be nearly linear), with a slight upturn at high galaxy masses. We also show the observed relation from Peng et al. (2008), which is also quite flat, opposed to the 'U'-shaped relation observed between the specific frequency and galaxy stellar mass or luminosity. The normalization of our fiducial model is also quite close to that of the Peng et al. observational sample.

As discussed in Peng et al. (2008, highlighted in their fig. 6), the 'U' shape observed in the relation between the specific frequency (S_N) and galaxy luminosity (M_z) corresponds to a much flatter relation between specific mass (S_M) and galaxy stellar mass ($M_\star$) due to the mean GC luminosity decreasing with galaxy luminosity. We chose to compare our models with the observed S$_M$–$M_\star$ relation, rather than in specific frequency due the sensitivity of S$_N$ on the shape of the GC mass function at low masses. As E-MOSAICS underestimates cluster disruption, in particular at lower masses, the total mass in GCs is expected to be more robust than the number of GCs.

H17 found an upward kink in the M_{GC}–$M_\star$ relation at a galaxy stellar mass of ~10^{10} M$_\odot$, implying that more massive galaxies have a higher fraction of their stellar mass in GCs than lower mass galaxies. Our fiducial simulations reproduce this upward kink and do so at a similar galaxy mass (see the top right panel in Fig. 1). Looking at the '$M_{c,\star}$ only' model, no such upward trend is seen, suggesting that the cause of the trend is due to a higher CFE in higher mass galaxies. We find that the upturn is also present when using the initial GC masses at high redshift (see Fig. 5), lending further credence to the CFE interpretation.

We note that the low-mass galaxies used in F18 are consistent with the S$_M$–$M_\star$ relation from Peng et al. (2008), hence are consistent with the results of the simulations presented here. Again, this argues that the differences between the observed and simulated M_{GC}–M_{halo} relations are driven by differences in the underlying $M_\star$–M_{halo} relation, and are not directly related to the GC population properties.

Looking at the other models that differ in their input GC formation physics in Fig. 1, we find that they also result in changes to the M_{GC}–$M_\star$ relation. If we adopt a model with a pure power-law mass function, but allow the CFE to vary, the resulting simulations do not reproduce the observed normalization and also display a trend with galaxy mass that is inconsistent with the observations. Alternatively, for a fixed CFE (10 per cent), but variable $M_{c,\star}$, the simulations reproduce the normalization of the S$_M$–$M_\star$ relation, but fails to reproduce the observed upturn at high halo masses.

4 DISCUSSION AND CONCLUSIONS

We have analysed the M_{GC}–M_{halo} relation realized in a large cosmological volume (34.4 cMpc on a side) simulated with the E-MOSAICS model, in order to establish the origin of the relation and its evolution over cosmic time, and to explore its sensitivity to the input physics of GC formation and disruption[5] Within the simulated volume, we follow the formation and evolution of the GC

population in 1707 galaxies with stellar masses above 10^8 M$_\odot$ at z = 0. In agreement with recent other models, such as Kruijssen (2015), El-Badry et al. (2019), and Choksi & Gnedin (2019), we find a linear M_{GC}–M_{halo} relation above a halo (M$_{200}$) mass of ~5 × 10^{11} M$_\odot$. This is driven essentially by the process of hierarchical galaxy growth through the central limit theorem.

Above ~5 × 10^{11} M$_\odot$, i.e. in the linear regime, we have investigated the effects that control the normalization, i.e. why $\eta \equiv M_{GC}/M_{halo} \sim 5 \times 10^{-5}$. Unlike most previous numerical models that had to set certain free parameters in order to reproduce this value, we are able to adjust the input physics directly to uncover the origin of the normalization. We find that not including an environmentally dependent term for the cluster formation efficiency (Γ) or the mass function exponential truncation ($M_{c,\star}$) leads to a systematic offset from the observations. Our fiducial model reproduces the observed value without adjusting any parameters. Likewise, we have investigated the role of cluster disruption in setting the normalization and have found that it plays a dominant role (as predicted by Kruijssen 2015). By not including GC disruption (which is dominated by tidal shocks) the normalization is off by a factor of ~10.

Our simulations predict a downturn in the M_{GC}–M_{halo} relation below ~5 × 10^{11} M$_\odot$. By changing the input physics of cluster formation, specifically Γ and $M_{c,\star}$, we show that the formation physics are unlikely to be the underlying cause of the downturn. Similarly, by looking at the simulation results with and without cluster mass-loss (through stellar evolution and the loss of stars from internal dynamics and external tidal effects), we show that cluster disruption is also unlikely to be the origin of the downturn. Instead, the cause of the downturn is the underlying relation between the stellar mass ($M_\star$) and halo mass (M_{halo}) of galaxies. By applying a range of $M_\star$–M_{halo} relations from the literature to observed samples of GC systems and their host galaxies, we show that the observations presented to date are consistent with the predicted downturn from our simulations.

Additionally, we show that satellite galaxies tend to scatter up and to the left in the η–M_{halo} relation, due to the fact that the dark matter halo is more extended than the stellar or GC population of a galaxy, so the dark halo is tidally stripped by the central galaxy before the GCs and stellar mass are. This results in a flatter η–M_{halo} relation, with the downturn being less pronounced. Along with the adopted $M_\star$–M_{halo} relation, this effect, as well as the exclusion of galaxies without GCs, may explain why observational studies to date have not found evidence of the predicted downturn. In order to definitively establish the form of the M_{GC}–M_{halo} relation at low galaxy masses, volume-complete sample of isolated galaxies that accounts for distance-dependent selection limits would be required.

We note that the results of Burkert & Forbes (2020), which use the number of observed GCs in galaxies as an indicator of their halo masses, is also sensitive to the adopted $M_\star$–M_{halo} relation. The use of the $M_\star$–M_{halo} relation from the EAGLE simulations (used in this work) would result in a turndown in the N_{GC}–M_{halo} at $M_{halo} \sim$ 5 × 10^{11} M$_\odot$, analogous to the M_{GC}–M_{halo} relation.

Importantly, when exclusively considering the baryonic properties of the galaxies (i.e. using a directly observable quantity such as stellar mass instead of halo mass), namely S$_M$ versus $M_\star$, we find good agreement between the simulations and observations. Our fiducial model reproduces the observed, (near-)linear M_{GC}–$M_\star$ relation, including its normalization. Since we expect a more

---

[5]We note that the fiducial E-MOSAICS model was originally designed and tested using a suite of 10 Milky Way-mass cosmological zoom-in simulations. The M_{GC}–M_{halo} relations presented here apply the identical model to a

complete cosmological volume, and the predicted trends with galaxy mass thus represent a genuine prediction.

direct relation between stellar clusters and the stellar component of their host galaxies, rather than with the dark matter halo, and acknowledging the fact that observations are generally restricted to the visible component of galaxies, we argue that the $M_{\rm GC}$–$M_\star$ relation is the more physically motivated relation between clusters and their host galaxy. We find that changing the cluster formation physics (i.e. fixing either the CFE or adopting an ICMF without a truncation mass) results in $M_{\rm GC}$–$M_\star$ relations clearly at odds with observations. Hence, this relation can be used as a powerful tool to test cluster population formation physics.

Our fiducial model also reproduces the observed upturn in the $M_{\rm GC}$–$M_\star$ relation at a galactic stellar mass of $\sim 10^{10}$ $M_\odot$. By exploring the behaviour of this relation in the different formation physics simulations, as well as its evolution with redshift (both for present-day GC masses and the initial values) we found that the upturn is caused by an increase in the median CFE for higher mass galaxies.

Finally, we predict a strong evolution in both the $M_{\rm GC}$–$M_{\rm halo}$ and $M_{\rm GC}$–$M_\star$ relations as a function of redshift. This is due to a combination of (1) GC formation and disruption over extended periods and (2) the continuous build up of galaxies for both the dark matter and stellar components. Initial observational evidence for this evolution has been identified by inferring the masses of satellite galaxies accreted by the Milky Way over the past 10 Gyr (Kruijssen et al. 2020). Direct evidence may be obtained by directly observing (young) GC populations at high redshift.

DATA AVAILABILITY

The data underlying this article will be shared on reasonable request to the corresponding author.

REFERENCES

Adamo A., Bastian N., 2018, Astrophysics and Space Science Library, Vol. 424, The Birth of Star Clusters. Springer-Verlag, Berlin, p. 91
Bastian N., 2008, MNRAS, 390, 759
Behroozi P. S., Wechsler R. H., Conroy C., 2013, ApJ, 770, 57
Behroozi P., Wechsler R. H., Hearin A. P., Conroy C., 2019, MNRAS, 488, 3143
Blakeslee J. P., 1999, AJ, 118, 1506
Blakeslee J. P., Tonry J. L., Metzger M. R., 1997, AJ, 114, 482
Booth C. M., Schaye J., 2009, MNRAS, 398, 53
Boylan-Kolchin M., 2017, MNRAS, 472, 3120
Burkert A., Forbes D. A., 2020, AJ, 159, 56
Choksi N., Gnedin O. Y., 2019, MNRAS, 488, 5409
Cook D. O. et al., 2012, ApJ, 751, 100
Crain R. A. et al., 2015, MNRAS, 450, 1937
Davis M., Efstathiou G., Frenk C. S., White S. D. M., 1985, ApJ, 292, 371
Dolag K., Borgani S., Murante G., Springel V., 2009, MNRAS, 399, 497
El-Badry K., Quataert E., Weisz D. R., Choksi N., Boylan-Kolchin M., 2019, MNRAS, 482, 4528
Forbes D. A., Alabi A., Romanowsky A. J., Brodie J. P., Strader J., Usher C., Pota V., 2016, MNRAS, 458, L44
Forbes D. A. et al., 2018a, Proc. R. Soc. A, 474, 20170616
Forbes D. A., Read J. I., Gieles M., Collins M. L. M., 2018b, MNRAS, 481, 5592 (F18)
Georgiev I. Y., Puzia T. H., Goudfrooij P., Hilker M., 2010, MNRAS, 406, 1967
Gieles M., Baumgardt H., 2008, MNRAS, 389, L28
Gnedin O. Y., Hernquist L., Ostriker J. P., 1999, ApJ, 514, 109
Harris W. E. et al., 2014, ApJ, 797, 128
Harris W. E., Blakeslee J. P., Harris G. L. H., 2017, ApJ, 836, 67
Holtzman J. A. et al., 1992, AJ, 103, 691
Hudson M. J., Harris G. L., Harris W. E., 2014, ApJ, 787, L5
Hughes M. E., Pfeffer J., Martig M., Bastian N., Crain R. A., Kruijssen J. M. D., Reina-Campos M., 2019, MNRAS, 482, 2795
Hughes M. E., Pfeffer J. L., Martig M., Reina-Campos M., Bastian N., Crain R. A., Kruijssen J. M. D., 2020, MNRAS, 491, 4012
Jahnke K., Macciò A. V., 2011, ApJ, 734, 92
Johnson T. L. et al., 2017, ApJ, 843, L21
Jordán A. et al., 2007, ApJS, 171, 101
Kruijssen J. M. D., 2012, MNRAS, 426, 3008
Kruijssen J. M. D., 2014, Class. Quantum Gravity, 31, 244006
Kruijssen J. M. D., 2015, MNRAS, 454, 1658
Kruijssen J. M. D., Pelupessy F. I., Lamers H. J. G. L. M., Portegies Zwart S. F., Icke V., 2011, MNRAS, 414, 1339
Kruijssen J. M. D., Pfeffer J. L., Crain R. A., Bastian N., 2019a, MNRAS, 486, 3134
Kruijssen J. M. D., Pfeffer J. L., Reina-Campos M., Crain R. A., Bastian N., 2019b, MNRAS, 486, 3180
Kruijssen J. M. D. et al., 2020, MNRAS, preprint (arXiv:2003.01119)
Mackey D. et al., 2019, Nature, 574, 69
Mistani P. A. et al., 2016, MNRAS, 455, 2323
Moster B. P., Naab T., White S. D. M., 2013, MNRAS, 428, 3121
Moster B. P., Naab T., White S. D. M., 2018, MNRAS, 477, 1822
Peng E. W. et al., 2008, ApJ, 681, 197
Pfeffer J., Kruijssen J. M. D., Crain R. A., Bastian N., 2018, MNRAS, 475, 4309
Pfeffer J., Bastian N., Kruijssen J. M. D., Reina-Campos M., Crain R. A., Usher C., 2019, MNRAS, 490, 1714
Planck Collaboration XVI, 2014, A&A, 571, A16
Prieto J. L., Gnedin O. Y., 2008, ApJ, 689, 919
Reina-Campos M., Kruijssen J. M. D., 2017, MNRAS, 469, 1282
Reina-Campos M., Kruijssen J. M. D., Pfeffer J., Bastian N., Crain R. A., 2018, MNRAS, 481, 2851
Reina-Campos M., Kruijssen J. M. D., Pfeffer J. L., Bastian N., Crain R. A., 2019, MNRAS, 486, 5838 (RC19)
Reina-Campos M., Hughes M. E., Kruijssen J. M. D., Pfeffer J. L., Bastian N., Crain R. A., Koch A., Grebel E. K., 2020, MNRAS, 493, 3422

Rosas-Guevara Y. M. et al., 2015, MNRAS, 454, 1038

Schaye J., Dalla Vecchia C., 2008, MNRAS, 383, 1210

Schaye J. et al., 2015, MNRAS, 446, 521

Schechter P., 1976, ApJ, 203, 297

Schweizer F., Seitzer P., 1998, AJ, 116, 2206

Spitler L. R., Forbes D. A., 2009, MNRAS, 392, L1

Springel V., 2005, MNRAS, 364, 1105

Springel V., White S. D. M., Tormen G., Kauffmann G., 2001, MNRAS, 328, 726

Usher C., Pfeffer J., Bastian N., Kruijssen J. M. D., Crain R. A., Reina-Campos M., 2018, MNRAS, 480, 3279

Usher C., Brodie J. P., Forbes D. A., Romanowsky A. J., Strader J., Pfeffer J., Bastian N., 2019, MNRAS, 490, 491

van de Voort F., Schaye J., Booth C. M., Dalla Vecchia C., 2011, MNRAS, 415, 2782

Vanzella E. et al., 2017, MNRAS, 467, 4304

Wiersma R. P. C., Schaye J., Smith B. D., 2009a, MNRAS, 393, 99

Wiersma R. P. C., Schaye J., Theuns T., Dalla Vecchia C., Tornatore L., 2009b, MNRAS, 399, 574

APPENDIX A: GC SELECTION

In this study, we determine the total mass of the GC population (M_{GC}) of a galaxy as the sum of the top two decades of mass within the cluster system. We adopt this approach rather than using a fixed mass limit (e.g. all mass above 10^5 M$_\odot$), because it is more likely to approximate GC selection in observational surveys. Observations of GC systems have a wide range of completeness limits, with some Local Group studies being complete to below 10^4 M$_\odot$ (e.g. F18, and
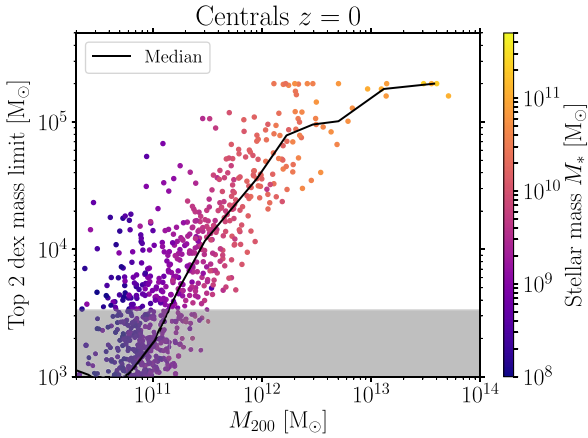

Figure A1. The lower limit of the mass range of our integration for each of the cluster populations in our study. For the total mass in GCs (M_{GC}), we restrict our integration to only the top two decades in mass of the cluster population (or slightly more if the lower limit of the integration exceeds 2×10^5 M$_\odot$). The solid black line shows the median mass limit as a function of M_{200}. The shaded region shows where the lower mass limit goes below our minimum initial cluster mass limit of 5×10^3 M$_\odot$ (descreased by a factor 0.67 to approximately account for stellar evolutionary mass-loss).
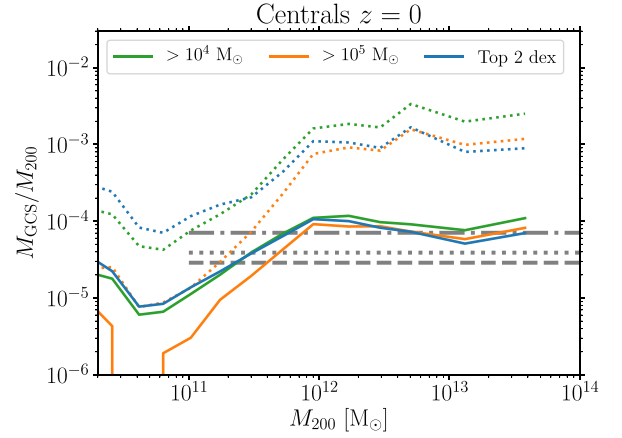

Figure A2. The M_{GC}–M_{halo} relation for different definitions of M_{GC} using different lower GC mass limits. The dotted lines show the results for the initial GC masses (with a lower limit 1.5 times that of the limit for evolved cluster masses, to account for stellar evolutionary mass-loss) and the solid lines show the results for $z = 0$ and including cluster disruption. Due to the disruption of low-mass clusters, the results are not strongly affected by the choice in the limit of defining GC mass within the simulations.

references therein), in fact in some cases the most massive cluster is below 10^4 M$_\odot$. In these and similar cases, using GCs only above a fixed limit will remove a large fraction of the GC mass within these systems. Other studies, focusing on massive central galaxies at 100–200 Mpc, are complete only to around the turnover of the GC mass or luminosity function or above (10^5–10^6 M$_\odot$; Harris et al. 2014). One exception to our definition above is that we do not let the lower mass limit of the integration go above 2×10^5 M$_\odot$, similar to the GC turnover mass in $>10^{11}$ M$_\odot$ galaxies (Jordán et al. 2007; Harris et al. 2014).

We do not make any cuts on metallicity, age, or galactocentric distance unless explicitly mentioned in the text.

In Fig. A1, we show the resulting lower mass limit for M_{GC} for each of the galaxies in our sample. The median mass limit is a strong function of the galaxy's stellar or halo mass, reaching $<2 \times 10^3$ M$_\odot$ for haloes with $M_{200} < 10^{11}$ M$_\odot$ and $>10^5$ M$_\odot$ for haloes $M_{200} > 2 \times 10^{12}$ M$_\odot$. At $M_{200} > 10^{13}$ M$_\odot$, the mass limits reach our adopted minimum of 2×10^5 M$_\odot$.

We explore the results of adopting a fixed mass limit, which are qualitatively largely similar to our variable limit, in Fig. A2. At halo masses $M_{200} > 10^{12}$ M$_\odot$, our results are insensitive to the mass limit adopted. At halo masses $M_{200} < 10^{12}$ M$_\odot$, adopting a mass limit of 10^5 M$_\odot$ would impart an artificial downturn in the M_{GC}–M_{halo} relation, due to low-mass galaxies forming few very massive GCs. Note that the upturn at $M_{200} \lesssim 4 \times 10^{10}$ M$_\odot$ is due to the fixed stellar mass selection of $M_* > 10^8$ M$_\odot$.

This paper has been typeset from a TeX/LaTeX file prepared by the author.